Comparison of crash simulations on two types of flying cars

Hiroto Sato[1[0009-0009-1659-2809]], Ayato Takii[2[0000−0003−3257−7640]], Masashi Yamakawa[1[0000−0001−5960−2602]], Yusei Kobayashi[1[0000−0002−5690−2033]], Shinichi Asao[3[0000−0003−4326−8480]], Seiichi Takeuchi[3] and Takahiro Ikeda[1[0009−0008−7496−9056]]

[1]Kyoto Institute of Technology, Hashikami, Matsugasaki, Sakyo, Kyoto 606-8585, Japan
[2] Kobe University, 1-1 Rokkodaicho, Nada-Ku, Kobe, Hyogo 657-8501, Japan
[3] College of Industrial Technology, Nishikoya, Amagasaki, Hyogo 661-0047, Japan
m4623016@kit.edu.ac.jp

Abstract. Numerical simulations are being used to ensure safety in the development of flying cars, which are expected to solve all kinds of traffic problems. In order to reproduce flight in a virtual environment, this research has been conducting numerical simulation research using the moving computational domain method and the multi-axis sliding mesh method to calculate the coupling of fluid and rigid body motion. This method enables rotational motion of the rotor and flight in an infinite region, and visualization of the flow field around the aircraft and its behavior including control. In this study, a comparison of the behavior during sudden rotor stops was performed on two different aircraft: the coaxial contra-rotating octorotor eVTOL treated in a previous study and a newly modeled domed dodecarotor eVTOL. The increased number of rotors and the wider circular arrangement of the rotors allowed for a wider range of measures to be taken in the event of rotor stoppage, and the crash risk was reduced by a factor of approximately 1/100. The differences in crash conditions and changes in aircraft attitude based on a comparison of the two models indicate that this calculation method allows for design improvements and behavior prediction based on relative evaluation.

Keywords: Computational Fluid Dynamics, Advanced Air Mobility, Crash.

1 Introduction

In recent years, increasing attention has been directed toward utilizing low-altitude airspace—currently characterized by relatively low usage density—as a new mode of personal transportation. This has led to the growing interest in so-called "flying cars," also known as Advanced Air Mobility (AAM). Among them, electric vertical takeoff and landing aircraft (eVTOL), which require no runways and offer potential advantages in terms of convenience and environmental impact [1], are especially noteworthy. However, since these vehicles are intended to operate over urban areas, safety remains the most critical concern. In fact, mechanical failures account for approximately 15% of all

ICCS Camera Ready Version 2025
To cite this paper please use the final published version:
DOI: 10.1007/978-3-031-97635-3_4

accidents involving small aircraft and helicopters, with over 50% of such incidents resulting in fatalities [2], highlighting the serious risks posed by component failures.

To improve development efficiency, a variety of numerical simulation techniques have been proposed. Prior studies have made significant progress in this field: Jun-Young An et al. [3] analyzed aircraft performance using dynamic modeling, while Okazaki et al. [4] investigated control strategies for small drones. Further research has explored turning maneuvers and attitude changes during abrupt rotor stoppage [5][6][7], demonstrating the importance of coupling dynamic and fluid models. However, these studies have primarily focused on a single vehicle model, limiting the ability to evaluate differences in aircraft characteristics or to validate simulation results against real-world behavior.

To address this gap, the present study conducts simulations of abrupt rotor stoppage in a larger eVTOL model with increased rotor count, size, and weight. By comparing the flight behavior and attitude response during crash scenarios across different vehicle configurations, this research aims to quantitatively assess the impact of rotor count on crash risk and attitude controllability.

2 Numerical Approach

2.1 Governing Equation

The Reynolds number at the tip of the propeller during hovering of the aircraft considered in this study is approximately 5.98×10^8, and the maximum Mach number is approximately 0.52.Therefore, the fluid is treated as a compressible fluid, and the 3-D Euler equation for a non-viscous compressible fluid and the equation of state for an ideal gas are used to prioritize computational efficiency and to avoid consideration of viscosity. The governing equations for the fluid are shown in Equations (1)-(3).

$$\frac{\partial \boldsymbol{q}}{\partial t}+\frac{\partial \boldsymbol{E}}{\partial x}+\frac{\partial \boldsymbol{F}}{\partial y}+\frac{\partial \boldsymbol{G}}{\partial z}=0, \tag{1}$$

$$\boldsymbol{q}=\begin{bmatrix}\rho\\ \rho u\\ \rho v\\ \rho w\\ e\end{bmatrix}, \boldsymbol{E}=\begin{bmatrix}\rho u\\ \rho u^2+p\\ \rho uv\\ \rho uw\\ u(e+p)\end{bmatrix}, \boldsymbol{F}=\begin{bmatrix}\rho v\\ \rho uv\\ \rho v^2+p\\ \rho vw\\ v(e+p)\end{bmatrix}, \boldsymbol{G}=\begin{bmatrix}\rho w\\ \rho uw\\ \rho vw\\ \rho w^2+p\\ w(e+p)\end{bmatrix}, \tag{2}$$

$$p=(\gamma-1)\left\{e-\frac{1}{2}\rho(u^2+v^2+w^2)\right\}. \tag{3}$$

Where $\boldsymbol{q}$ is the conserved quantity vector, $\boldsymbol{E}$, $\boldsymbol{F}$, and $\boldsymbol{G}$ are the inviscid flux vectors in the x, y, and z directions. ρ is the density of the fluid, u, v, and w are velocity components in the x, y, and z directions, p is the pressure of the gas, e is the total energy per unit volume, and γ is the specific heat ratio. All variables are dimensionless quantities. Moreover, to reproduce the motion of a flying car through a weakly coupled fluid-rigid-body calculation, the three-dimensional Newton-Euler equations of motion for translation and rotation are used.

ICCS Camera Ready Version 2025
To cite this paper please use the final published version:
DOI: 10.1007/978-3-031-97635-3_4

2.2 Computational Conditions

To simulate the flight of a flying car under complex conditions, we coupled flight dynamics and fluid dynamics as in Takahashi et al [7], and used the MCD (Moving Computational Domain) method [8][9] and the multi-axis sliding mesh method [10]. Table 1 shows the characteristic values used to nondimensionalize the calculations. The characteristic length is the total length of the aircraft, the characteristic density is the air density, and the characteristic velocity is the speed of sound. The boundary conditions are slip wall boundary for the airframe surface, a Riemann boundary condition for the outer region, and sliding mesh interface boundary for the split interface.

Table 1. Characteristic values

Density of the air	1.247 kg/m^3
Characteristic velocity	340.29 m/s
Characteristic length	13.0 m

3 Flight Simulation of Flying Car

3.1 Computational Model

Fig.1 shows the computational model of the octorotor eVTOL with four pairs of coaxial contra-rotating rotors used in the previous study and the dodecarotor eVTOL with 12 rotors arranged in a dome shape that will be compared in this study. Table 2 shows the characteristics of the newly introduced model. The new model is considerably larger than the model used in the previous study. One rotor has three blades, and the smallest grid is in front of the rotor blade blades, with a minimum grid width of 6 mm as in the previous study. The computational model used in this study is an unstructured tetrahedral mesh and was created using MEGG3D [11][12]. The total number of elements is approximately 5.8 million, and these are computed in an OpenMP parallel environment [13]. The time step size for each step was set to 0.0005, and the total simulated duration was approximately 6 seconds. Using an Intel Core i9-14900K processor, the computation time required for simulating approximately 5 seconds of real time was about 18 days per case.

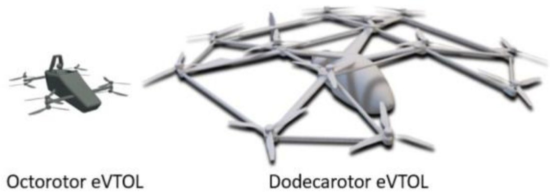

Fig.1. Computational Model for octorotor eVTOL and dodecarotor eVTOL

Table 2. Comparison of Aircraft Specifications

	octorotor eVTOL	dodecarotor eVTOL
Overall length and width [m]	4 × 4	13 × 13
Airframe weight [kg]	400	1400
Number of rotors [-]	8	12

ICCS Camera Ready Version 2025
To cite this paper please use the final published version:
DOI: 10.1007/978-3-031-97635-3_4

3.2 Flight Simulation Conditions

To outline this simulation, rotors are named as shown in Fig.2. First, the 12 rotors are roughly classified into three groups of three rotors each, FL (Front Left) FR, RL, and RR. The rotors with the greatest influence in the pitch direction are classified as 1, those with the greatest influence in the roll direction are classified as 2, and those with the greatest influence in the altitude direction are classified as 3. The direction of rotation is distinguished by color.

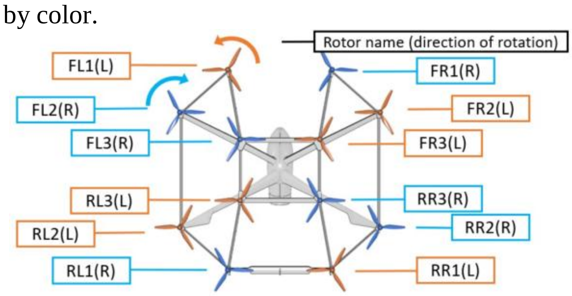

Fig.2. Rotor name of dodecarotor eVTOL

We will compare crash conditions and changes in aircraft attitude for two different aircraft models. For this purpose, a simulation was first conducted in which some of the rotors of the new aircraft were stopped suddenly while hovering. The combinations of rotors to be stopped are shown in Table 3. After that, we maintain hovering by PID control and mixing. The results will be compared with those of previous studies [7].

Table 3. Experimental conditions

terms	Rotor name to be stopped	Number of rotors to be stopped
(1)	FL1	1
(2)	FL	3
(3)	FL, RR	6
(4)	FL, FR3, RR	7
(5)	FL, FR3, RR, RL3	8
(6)	FL, FR1	4

4 Calculation Results

4.1 Comparison of one rotor stopped

A comparison is made between the FLU rotor stop in the coaxial contra-rotating octorotor eVTOL and the FL1 rotor stop in the dodecarotor eVTOL. Fig.3 shows the aircraft attitudes and torques over time after rotor stoppage. Solid lines represent octorotor eVTOL 1, and dotted lines represent dodecarotor eVTOL 2. The dodecarotor exhibits attitude changes reduced by a factor of eight or less but experiences greater vibration during hovering. This is likely due to its larger fuselage and longer propellers, which

ICCS Camera Ready Version 2025
To cite this paper please use the final published version:
DOI: 10.1007/978-3-031-97635-3_4

cause higher torque and blade tip speeds. The coaxial octorotor reduces vibration by lowering its rotational speed, made possible by thrust recovery from the lower propeller utilizing the upper propeller's wasted energy[14]. Furthermore, the rotor stop positions differ—about 1:1 from the center of gravity for the octorotor and 2:1 for the dodecarotor—which clearly affects the resulting moment and aircraft motion. These results demonstrate that aircraft structure and rotor layout significantly influence stability and vibration. Moreover, the effect of rotor placement is clearly reflected in the generated moments and aircraft behavior, indicating that the outcomes are reproducible even across different aircraft types.

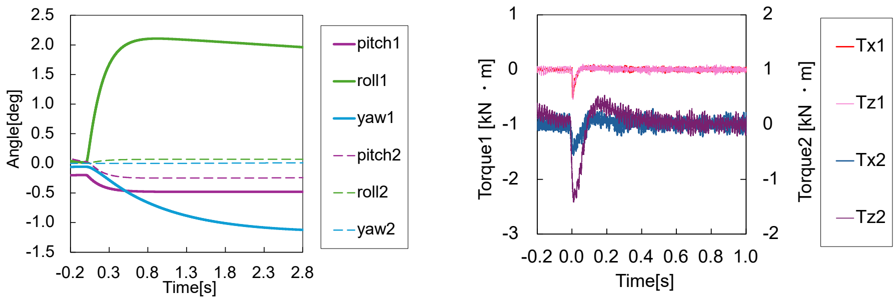

Fig.3. Comparison of fuselage attitude and torque around fuselage

4.2 Comparison of crashes due to sudden rotor stoppage

In the octocopter-type eVTOL, the aircraft crashed when the FLU and FLL rotors were suddenly stopped. Based on this, two failure conditions are examined for the dodecacopter-type eVTOL: (2) simultaneous stoppage of three front-left (FL) rotors, and (3) stoppage of an additional rotor on top of Condition (2). Fig. 4 shows the time histories of attitude changes and overlaid snapshots during descent for all three conditions. The solid line represents the octocopter (1), and the dashed line the dodecacopter (2). Q-criterion isosurfaces (second invariant of the velocity gradient tensor) are shown for both configurations: octorotor (left) and dodecarotor (right). These are colored by velocity magnitude, while the aircraft surfaces are colored by pressure. All values are non-dimensional.

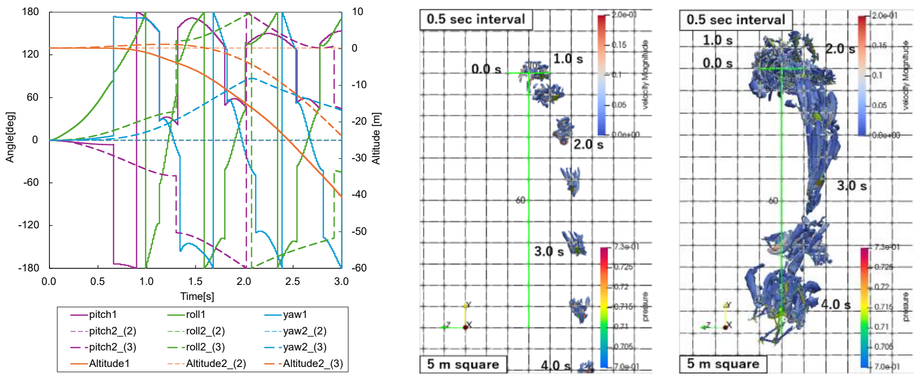

Fig.4. Time history of aircraft attitude changes and Sequential images

ICCS Camera Ready Version 2025
To cite this paper please use the final published version:
DOI: 10.1007/978-3-031-97635-3_4

In the dodecarotor eVTOL, Condition (2) maintained stable altitude, indicating successful hover, while the other conditions resulted in crashes. This suggests that even with front-left rotors stopped, attitude control remains possible due to four surrounding rotors (FR1, FR2, RL1, RL2) generating compensating moments near the center of gravity.

Comparing crash behaviors, the dodecarotor showed less attitude disturbance. Within 3 seconds, the octorotor rotated 3.5 times and dropped 40 m, whereas the dodecarotor rotated only 0.75 times and dropped 25 m. Assuming that all rotors fail independently with equal probability ppp, the crash probabilities are $\frac{1}{7}p^2$ and $\frac{8}{495}p^2$ for the octorotor and dodecarotor, respectively. These results demonstrate that increasing rotor count and distributing them circularly improves stability and greatly reduces crash risk in the event of rotor failures.

4.3 Summary of Rotor Sudden Stop in dodecarotor eVTOL

From conditions (1)-(6), we summarize the possibility of crashes depending on the number and location of rotor stops. First, it was found that up to three rotor stoppages, no combination of rotors would cause a crash, while four to six rotor stoppages would lead to a crash if the stoppages were unevenly located. When more than seven rotors were stopped, the aircraft was able to maintain its attitude; however, it could not sustain its altitude, leading to a crash.

From these results, we calculate the combination of rotor stoppages that lead to crashes and the probability of this aircraft crashing due to rotor stoppage by assuming that the probability of one rotor stoppage is p and constant. The results are summarized in Table 4.

Table 4. Combination of stop rotor arrangement to crash

Number of stopped rotors	0-3	4	5	6	7	8	9	10	11	12
combination	0	8	60	78	792	495	220	66	12	1
Probability of a crash	0	$\frac{8}{495}p^4$	$\frac{60}{792}p^5$	$\frac{78}{924}p^6$	p^7	p^8	p^9	p^{10}	p^{11}	p^{12}

The likelihood of a crash due to rotor stoppage can be estimated based on rotor-generated lift. Although four rotors can theoretically maintain attitude control—as seen in conventional quadcopters—greater lift is needed for heavier eVTOLs. Analysis showed that with four rotors operating at 169% of their hover speed, lift could balance aircraft weight within the control range. However, experiments revealed that even five functioning rotors failed to maintain hover. This discrepancy is attributed to rotor deceleration variations, strut interference, and aerodynamic effects that reduce actual lift. Once the aircraft tilts beyond a certain angle, sufficient lift can no longer be produced, revealing the limitations of multirotor systems under sudden changes. These findings validate the experiment. From Table 4, the probability that the dodecarotor eVTOL

ICCS Camera Ready Version 2025
To cite this paper please use the final published version:
DOI: 10.1007/978-3-031-97635-3_4

crashes due to rotor failures corresponds to the sum of the probabilities in the bottom row. Given that all terms are positive and the individual probability p is sufficiently small compared to 1, the arithmetic-geometric mean inequality can be applied. As a result, the total crash probability is obtained as $0.361p^8$.

4.4 Comparison of crash probabilities

Similarly, for octorotor eVTOL, let p denote the probability of a single rotor failure. Since a crash occurs when both rotors in a coaxial pair fail, the total crash probability is calculated as $0.658p^5$. While coaxial contra-rotating rotors offer compact and efficient assembly, failure in a coaxial pair significantly increases crash risk. In the dodecarotor eVTOL, even with a front-left rotor failure, attitude control is possible due to the symmetrical placement of four other rotors around the center of gravity. However, circular rotor arrangements tend to be larger and heavier, presenting a tradeoff between safety and performance. To contextualize risk, we compare with commercial airplanes, where the fatal accident rate is 1 in 13.7 million[15]. Assuming 10-hour flights, the accident rate is 7.3×10^{-6} per 1,000 hours, with 21% due to mechanical failures[16]. Given that airplanes carry 100 times more passengers, the acceptable crash probability due to rotor failure in flying cars is 1.53×10^{-8}. To match this safety level, dodecarotor rotor failure probability must be under $0.03\ [/1000 hours]$, and $0.00033\ [/1000 hours]$ for octorotors. These values serve as rotor design targets to ensure safety equivalent to that of airplanes.

5 Conclusions

Using coupled fluid–rigid body simulations with MCD and sliding mesh methods, we analyzed the effects of sudden rotor stoppages in a domed dodecarotor eVTOL, incorporating attitude control. Various rotor failure combinations were evaluated under hovering conditions, and comparisons were made with other aircraft, including a coaxial octorotor model. The simulations showed that hovering was maintainable with up to three rotors stopped, and in some cases, even with four to six, depending on their positions. This enabled a quantitative evaluation of crash probability. Theoretical lift calculations and experimental results also highlighted the limitations of multi-rotor systems in responding to sudden lift loss, particularly under aerodynamic interference.

Compared to the coaxial octorotor model from prior research, the dodecarotor's greater number of rotors and circular layout enabled more failure-tolerant configurations, significantly reducing crash risk by about 1/100. The study also revealed differences in crash dynamics and control behavior stemming from rotor placement and fuselage geometry. This simulation approach proved effective in reproducing emergency conditions and provided a practical tool for improving design reliability and predicting behavior under failure scenarios.

Acknowledgments. This paper is based on results obtained from a project, JPNP14004, subsidized by the New Energy and Industrial Technology Development Organization (NEDO).

ICCS Camera Ready Version 2025
To cite this paper please use the final published version:
DOI: 10.1007/978-3-031-97635-3_4

References

1. Ison, D.C.: Consumer willingness to fly on advanced air mobility (AAM) electric vertical takeoff and landing (eVTOL) aircraft. In: Collegiate Aviation Review International 2024, vol. 42, no. 1, pp. 103-118. https://doi.org/10.22488/okstate.24.100223 (2024)
2. Kunimitsu, I., Tatsuo, O.: Statistical Data Analyses on Aircraft Accidents in Japan: Occurrences, Causes and Countermeasures. In: American Journal of Operations Research, vol.5 no.3, pp. 222-245. http://dx.doi.org/10.4236/ajor.2015.53018 (2015)
3. An, J.-Y. et al.: Practical Approach to Mission Autonomy of Multiple Unmanned Air Mobilities. In: International Journal of Control, Automation, and Systems, vol. 22, no. 8, pp. 2513–2536. https://doi.org/10.1007/s12555-023-0662-6 (2024)
4. Okazaki, H., Isogai, K.: Motor Failure Issues in Flying Drones. In: IEICE Fundamentals Review, vol. 14, no. 1, pp. 44–59. https://doi.org/10.1587/essfr.14.1_44 (2020)
5. Gomi, R. et al.: Flight simulation from takeoff to yawing of eVTOL airplane with coaxial propellers by fluid-rigid body interaction. In: Advances in Aerodynamics, 5(1), (2023).
6. Magata, T., Takii, A., Yamakawa, M., Takeuchi, S., Chung, Y.M.: Forward and turning flight simulation of flying cars and comparative evaluation of flight dynamics models considering wind disturbances. In: Journal of Computational Science, 85, 102519, (2025)
7. Takahashi, N. et al.: Numerical Simulation of the Octorotor Flying Car in Sudden Rotor Stop. In: ICCS 2023, pp. 33-46 . (2023)
8. Yamakawa, M. et al.: Numerical Simulation for a Flow around Body Ejection using an Axisymmetric Unstructured Moving Grid Method, Computational Thermal Sciences, Vol.4, No.3, pp.217-223(2012)
9. Asao, S., Matsuno, K., Yamakawa, M.: Simulations of a falling sphere with concentration in an infinite long pipe using a new moving mesh system. In: Applied Thermal Engineering, 72(1), pp. 29–33, (2014)
10. Takii, A. et al.: Six degrees of freedom flight simulation of tilt-rotor aircraft with nacelle conversion. Journal of Computational Science, 44, 101164 (2020).
11. Ito, Y., Nakahashi, K.: Surface triangulation for polygonal models based on CAD data. In: International Journal for Numerical Methods in Fluids, 39(1), 75-96 (2002).
12. Ito, Y.: Challenges in unstructured mesh generation for practical and efficient computational fluid dynamics simulations. Comput Fluids 85(1):47–52 (2013).
13. Yamakawa, M. et al.: Domain decomposition method for unstructured meshes in an OpenMP computing environment. In: Computers and Fluids, 45(1), pp. 168–171 (2011)
14. Theys, B. et al.: Influence of propeller configuration on propulsion system efficiency of multi-rotor Unmanned Aerial Vehicles. In: 2016 ICUAS, pp. 1-9. IEEE. (2016).
15. Barnett, A. et al.: Airline safety: Still getting better? In: Journal of Air Transport Management, vol. 119, article 102641. https://doi.org/10.1016/j.jairtraman.2024.102641 (2024)
16. Khadivar, H. et al.: Flying safe: The impact of corporate governance on aviation safety. In: Journal of Air Transport Management, vol. 124, article 102743. (2025)

DOI: 10.1007/978-3-031-97635-3_4